

RESEARCH

Open Access



Introducing new plan evaluation indices for prostate dose painting IMRT plans based on apparent diffusion coefficient images

Saman Moradi¹, Bijan Hashemi^{1*} , Mohsen Bakhshandeh² , Amin Banaei¹ and Bahram Mofid³

Abstract

Background: Dose painting planning would be more complicated due to different levels of prescribed doses and more complex evaluation with conventional plan quality indices considering uniform dose prescription. Therefore, we tried to introduce new indices for evaluating the dose distribution conformity and homogeneity of treatment volumes based on the tumoral cell density and relative volumes of each lesion in prostate IMRT.

Methods: CT and MRI scans of 20 male patients having local prostate cancer were used for IMRT DP planning. Apparent diffusion coefficient (ADC) images were imported to a MATLAB program to identify lesion regions based on ADC values automatically. Regions with ADC values lower than $750 \text{ mm}^2/\text{s}$ and regions with ADC values higher than 750 and less than $1500 \text{ mm}^2/\text{s}$ were considered $\text{CTV}_{70\text{Gy}}$ (clinical tumor volume with 70 Gy prescribed dose), and $\text{CTV}_{60\text{Gy}}$, respectively. Other regions of the prostate were considered as $\text{CTV}_{53\text{Gy}}$. New plan evaluation indices based on evaluating the homogeneity (IOE(H)), and conformity (IOE(C)) were introduced, considering the relative volume of each lesion and cellular density obtained from ADC images. These indices were compared with conventional homogeneity and conformity indices and IOEs without considering cellular density. Furthermore, tumor control probability (TCP) was calculated for each patient, and the relationship of the assessed indices were evaluated with TCP values.

Results: IOE (H) and IOE (C) with considering cellular density had significantly lower values compared to conventional indices and IOEs without considering cellular density. ($P < 0.05$). TCP values had a stronger relationship with IOE(H) considering cell density ($R^2 = -0.415$), and IOE(C) without considering cell density ($R^2 = 0.624$).

Conclusion: IOE plan evaluation indices proposed in this study can be used for evaluating prostate IMRT dose painting plans. We suggested to consider cell densities in the IOE(H) calculation formula and it's appropriate to calculate IOE(C) without considering cell density values.

Keywords: Prostate cancer, Intensity-modulated radiotherapy, Radiobiology, Anatomical parameters, Algorithmic approach

Background

Modulated radiotherapy techniques such as intensity modulated radiotherapy (IMRT) and volumetric modulated arc therapy (VMAT) are among the most useful techniques for prostate radiotherapy [1], to deliver the prescribed dose to the target tissue and spare organs at risk (OARs) from irradiation. Although VMAT generally has a smaller treatment time and slightly better OAR sparing [2, 3], however, IMRT has indicated similar

*Correspondence: bhashemi@modares.ac.ir

¹ Department of Medical Physics, Faculty of Medical Sciences, Tarbiat Modares University, Tehran 1411713116, Iran
Full list of author information is available at the end of the article



© The Author(s) 2022. **Open Access** This article is licensed under a Creative Commons Attribution 4.0 International License, which permits use, sharing, adaptation, distribution and reproduction in any medium or format, as long as you give appropriate credit to the original author(s) and the source, provide a link to the Creative Commons licence, and indicate if changes were made. The images or other third party material in this article are included in the article's Creative Commons licence, unless indicated otherwise in a credit line to the material. If material is not included in the article's Creative Commons licence and your intended use is not permitted by statutory regulation or exceeds the permitted use, you will need to obtain permission directly from the copyright holder. To view a copy of this licence, visit <http://creativecommons.org/licenses/by/4.0/>. The Creative Commons Public Domain Dedication waiver (<http://creativecommons.org/publicdomain/zero/1.0/>) applies to the data made available in this article, unless otherwise stated in a credit line to the data.

outcomes to VMAT and also newer and more complicated radiotherapy techniques such as Tomotherapy [4–7].

One of the strategies to improve the efficiency of radiotherapy is increasing the prescribed dose in regions with higher cancer cell densities [8]. Higher doses ranging from 74 to 80 Gy has been reported to have improvements in the outcome of prostate cancer treatment [4–7, 9–14]. However, delivering these high doses is impossible using conventional radiotherapy without a significant probability of occurring severe radiation toxicities [14]. Modulated techniques (IMRT, VMAT, Tomotherapy) can reduce these toxicities by optimizing radiation conformation [15, 16].

The usual clinical protocol in prostate radiotherapy is to deliver a uniform dose to a defined planning target volume (PTV) [17]. Dose painting (DP) was introduced to increase the tumor local control rates by delivering higher dose levels to the regions with higher cellular densities or radioresistance tissues while sparing healthy tissue. It is designed to give additional doses to subvolumes with high radioresistance due to hypoxia or other reasons as quantified by functional imaging [18]. Higher dose levels in tumor nodules or dominant intraprostatic lesions can improve local control without increasing complication rates [4–7, 14, 15].

In dose painting, tumors and intra-tumoral lesions (with higher cell densities) are delineated based on multiparametric MRI, consisting of a T2-weighted (T2w), diffusion-weighted (DWI), apparent diffusion coefficient (ADC), and a dynamic contrast-enhanced (DCE) sequences [19, 20]. Other imaging modalities such as positron emission tomography (PET) with ^{18}F compounds (like ^{18}F -FDG, ^{18}F -choline, ^{11}C -choline and ^{18}F -Fluoromisonidazole) are also available and their applications were reported for delineating intra tumor lesions [21–24]. As an alternative to manual contouring, automated methods for the prostate have been developed [25–29].

The application of DP radiation therapy is increased in recent years. However, the aspects of plan evaluation remain controversial now [30]. For example, conventional indices, such as the conformity index (CI) and the homogeneity index (HI), commonly used in routine clinical practice for plan evaluation, are formulated based on the paradigm of uniform dose prescription. Therefore, these indices need to be modified for DP planning. There are few studies that modified these indices for use in DP plan evaluation [31–33]. In a study by Park et al. [31], they introduced a new plan quality index, named “index of achievement (IOA)”. Their introduced index assesses how close the planned dose distribution is to the

prescribed one considering the differences between the prescribed and the delivered dose for each voxel multiplied by the relative volume of the voxel in the target volume. Their index did not account for the importance of different lesions with different cellular densities or radioresistance properties and also need to be calculated by a computer program. We think that the plan evaluation index in DP planning must be easy to calculate without a computer program and accounts importance of different lesions inside target volume. Therefore, in this study we tried to propose new dose painting plan evaluation indices with simpler calculation methods incorporating cellular density as an index of lesion importance obtained from MRI diffusion images for prostate cancer IMRT.

Methods

This single-center retrospective study was performed in accordance with the national ethical guidelines and regulations. The national Ethics Committee has approved the methods of this study. MRI and CT images of patients were used in this study without any intervention in the diagnostic or treatment procedures. In addition, gathering the informed consent was waived because of the retrospective nature of the study.

Imaging data (CT and MRI scans) of 20 male patients having local prostate cancer who had no previous surgery, hormone therapy (AST or ADT), and prostate radiation therapy with at least one non-high risk intraprostatic lesion (IL) in stages of T1 to T3a, were used in this study. Patients’ ages ranged from 54 to 85 years, with a mean age of 69.4.

The CT (Matrix size: 512*512; Slice thickness: 3 to 5 mm), T2w-MRI (fast spin echo pulse sequence with TE: 80 ms and TR: 7800 ms), diffusion-weighted MRI (echo planar imaging with TE: 88 ms, and TR: 4600 ms) and apparent diffusion coefficient (fast spin echo pulse sequence with TE: 100 ms and TR: 3000 ms) images were taken using a Siemens 16-slice Emotion CT and a 1.5 Tesla Avanto MRI machine (Siemens Healthcare GmbH, Germany). The patients were placed in supine positions for both imaging procedures. Diffusion-weighted images (DWI) were gathered with three signals per image with a scattering-sensitive gradient in three orthogonal planes and b-values of 0, 250, 500, and 1000 s per square. DW-MRI images have a resolution of $1.64 \times 1.64 \times 3$ mm and a FOV of 210×210 mm, a matrix size of 128×128 pixels, and a NEX (number of excitation) parameter equal to four. Apparent diffusion coefficient (ADC) maps (images) were automatically calculated from DW-MRI images. ADC is a measure of the magnitude of water molecules diffusion within tissue [34], and can show the cellular density in some tumors like prostate [35].

CT and MRI images were combined using a rigid registration algorithm in the treatment planning software (TPS) based on bone landmarks, gold markers implanted in the prostate and skin surfaces, and then verified by a specialized physician. The MRI and CT registration were used to contour the lesion volumes inside the patients' prostate and radiation-sensitive organs. It also allows for more precise target volume delineation in prostate cancer patients [36].

An in-house MATLAB program was developed to automatically identify lesion regions on ADC images based on ADC values. The MATLAB code is available in the "Additional file 1" section. Two types of predominant lesions were considered in the prostate, one related to lesions with ADC values lower than $750 \text{ mm}^2/\text{s}$ (PTV-1), and the other was related to lesions with ADC values higher than 750 and less than $1500 \text{ mm}^2/\text{s}$ (PTV-2). The upper limit of ADC values in tumor tissues varies in different studies but usually was considered more than $1300 \text{ mm}^2/\text{s}$ [37]. In this study, the apparent diffusion coefficient threshold for distinguishing tumor tissue from normal prostate tissue was $1500 \text{ mm}^2/\text{s}$. The highest measurable value of ADC in MATLAB software was $5000 \text{ mm}^2/\text{s}$. The ADC images were imported to the MATLAB program, and the voxels in a specific range of ADC values were determined. The related voxels for determining areas must at least have a minimum number (400 voxels) located next to each other so that the software can identify those areas separately. Considering the relationship between Gleason score (GS) and ADC cut-off value based on a study by Pepe et al. [38], different target volumes were identified within the prostate. Each patient's output DICOM RS file was then transferred to the treatment planning system to contour these new structures (prostatic lesions) on the CT images. Contouring of other organs at risk (OARs) was performed by an experienced radiation oncologist in the treatment planning system.

Prescription dose levels, except in dominant intraprostatic lesions (DILs), were taken from the Jerezek-Fossa et al. study [39]. The upper limit for the prescribed dose for DIL was considered 70 Gy in 27 fractions for high risk DILs. This hypofractionated dose escalation was used and evaluated in many studies [40–47]. According to a study by Onjukka et al. [48], this hypofractionated dose was equivalent to 86 Gy in 37 sessions (used in the study of Uzan et al. [49]). A prescribed dose for DILs with lower risks was considered 66 Gy. The clinical target volume of the base of the seminal vesicles was considered $\text{CTV}_{53\text{Gy}}$. The planning target volume for this target ($\text{PTV}_{53\text{Gy}}$) was formed by adding eight millimeter isotropic margins to $\text{CTV}_{53\text{Gy}}$ in order to account for patient and equipment placement errors. The whole prostate

volume (except the DILs) was considered CTV_{60} ; similarly, $\text{PTV}_{60\text{Gy}}$ was formed by adding 5 mm margins to the $\text{CTV}_{60\text{Gy}}$. The margin was reduced to zero in the posterior region, where the target volume overlaps with the rectum. Two millimeters margins were added to $\text{CTV}_{66\text{Gy}}$ and $\text{CTV}_{70\text{Gy}}$ to create $\text{PTV}_{66\text{Gy}}$ and $\text{PTV}_{70\text{Gy}}$ without extending beyond $\text{CTV}_{60\text{Gy}}$ or overlapping with the rectum, bladder, and urethra due to the uncertainty in defining the DILs [49]. Furthermore, planning at risk volumes (PRVs) were created for high-risk organs, including the rectum, urethra, and bladder, with margins of two millimeters. The dose escalated DIL regions with the whole prostate were presented in Fig. 1. Furthermore, the procedure used to automatically contour the intraprostatic DILs is illustrated in Figs. 1-a and 1-b.

The IMRT plans were designed with Eclipse software (version 11, Varian Corporation, USA) for each patient. IMRT plan with nine coplanar fields in gantry angles of 0, 30, 60, 105, 140, 220, 260, 300, and 330 was designed to irradiate PTVs with prescribed doses. All the plans were interactively optimized based on our institutional planning protocol derived from a previous study by Pollak et al. [50]. The optimization algorithm was Dose Volume Optimizer (DVO) which is enclosed in Eclipse treatment planning software and clinically approved by previous studies [51]. The planning optimization objectives are presented in Table 1. An experienced physicist evaluated all the treatment plans to ensure compliance with reported dose constraints [52].

After treatment planning optimization, final dose calculations were performed by the anisotropic analytical algorithm (AAA) in the Eclipse software. The calculation accuracy of this algorithm was previously approved in several studies [53–55]. Dose volume histograms (DVHs) of the CTVs for each patient were entered in BioSuite software [56]. The tumor control probability (TCP) values were calculated using the Poisson model [57], based on radiobiological model parameters proposed by Deb and Fielding [58].

We introduced two indices of effectiveness (IOE) for evaluating IMRT dose painting plan dose distribution. One IOE can evaluate the conformity of CTVs, IOE(C), and another IOE can assess the overall dose distribution homogeneity of target volumes, IOE(H). The previous equation proposed by Park et al. [31] has relative volume coefficients, and these coefficients were included in our IOE equations accounting for the effect of each target (DIL) on the overall value of IOE. Furthermore, cell density values obtained from ADC maps were used in the IOE equations. The cell density is a measure of the clonogenicity level for each of the tumor volumes. The equations of IOE(H) and IOE(C) are as follows:

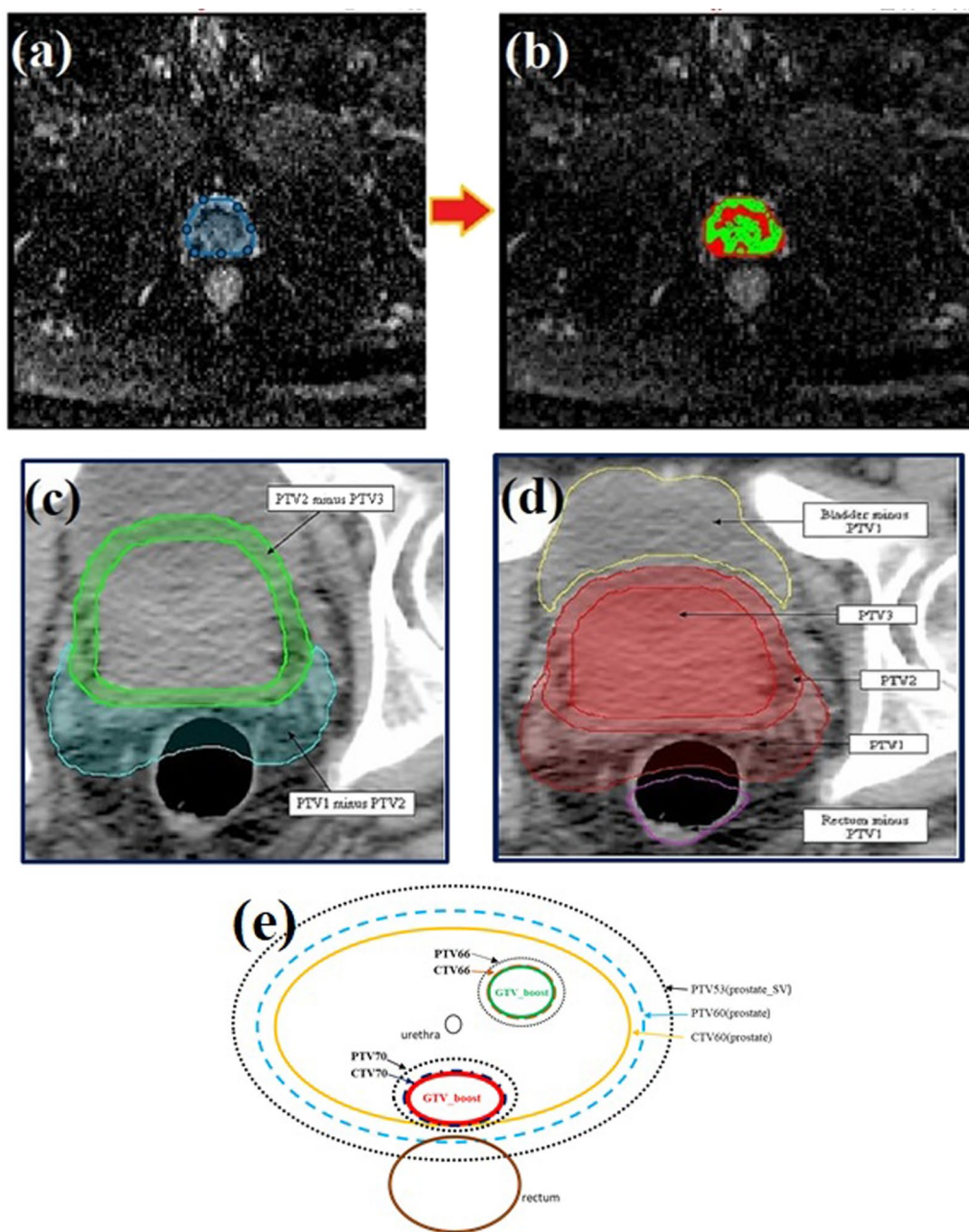


Fig. 1 The procedure used to automatically contour the intraprostatic dose-escalated DILs. **a** Delineating the whole prostate manually on ADC images. **b** Automatic contouring of different intraprostatic lesions based on ADC values. **c** Importing the contours from ADC images on registered CT images. **d** Determining DILs and margins to create different DILs with different dose levels on CT images. **e** Schematic of intraprostatic DILs and their PTVs with different dose levels

Table 1 The planning optimization objectives used for prostate dose painting IMRT

Structures	Objectives
Bladder	$V_{40.8\text{Gy}} < 50\%$
	$V_{48.6\text{Gy}} < 25\%$
	$V_{60\text{Gy}} < 5\%$
	Max dose < 65 Gy
Rectum	$V_{40.8\text{Gy}} < 50\%$
	$V_{48.6\text{Gy}} < 35\%$
	Max dose < 65 Gy
	$V_{60\text{Gy}} < 3\%$
Femoral heads	Max dose < 40 Gy
Bowel	$V_{50\text{Gy}} < 17\text{ cc}$
	Max dose < 60 Gy
PTVs	$V_{98\%} > 98\%$
	$V_{105\%} < 2\%$

* $V_{x\text{Gy}}$ represents the percentage of the structure volume received at least x Gy

* $V_{x\%}$ represents the percentage of the structure volume received at least x% of the prescribed dose

$$\begin{aligned}
 IOE(H) = & \left(HI_1 \times \frac{CD_1}{CD_p} \times \frac{V_1}{V_T} \right) \\
 & + \left(HI_2 \times \frac{CD_2}{CD_p} \times \frac{V_2}{V_T} \right) \\
 & + \left(HI_3 \times \frac{CD_3}{CD_p} \times \frac{V_3}{V_T} \right)
 \end{aligned} \tag{1}$$

$$\begin{aligned}
 IOE(C) = & \left(CI_1 \times \frac{CD_1}{CD_p} \times \frac{V_1}{V_T} \right) \\
 & + \left(CI_2 \times \frac{CD_2}{CD_p} \times \frac{V_2}{V_T} \right) \\
 & + \left(CI_3 \times \frac{CD_3}{CD_p} \times \frac{V_3}{V_T} \right)
 \end{aligned} \tag{2}$$

HI_1 , HI_2 , and HI_3 are the homogeneity indices for $CTV_{70\text{Gy}}$, $CTV_{66\text{Gy}}$, and $CTV_{60\text{Gy}}$ respectively. Similarly, the CI_1 , CI_2 , and CI_3 are the conformity indices for $CTV_{70\text{Gy}}$, $CTV_{66\text{Gy}}$, and $CTV_{60\text{Gy}}$ respectively. V_1 , V_2 , and V_3 are the volumes, and CD_1 , CD_2 , and CD_3 are the cell density of these CTVs. In addition, V_T and CD_p are the total volume and mean cell density value of the whole CTV (sum of all CTVs).

Furthermore, the $IOE(C)$ and $IOE(H)$ were calculated without considering the cell density, and they were compared with IOE indices considering cell density (our proposed indices) and also the mean of the conventional HI and CI values. Equations related to IOE indices without considering cell densities and the mean of conventional indices are presented in Eqs. 3–6.

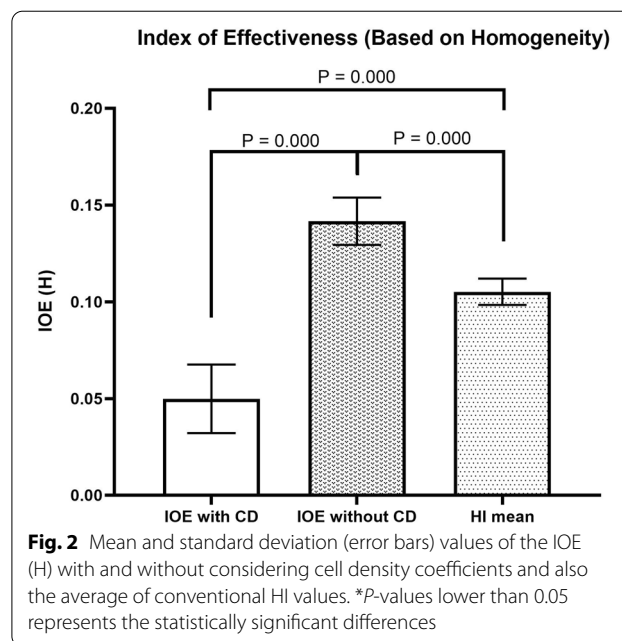


Fig. 2 Mean and standard deviation (error bars) values of the $IOE(H)$ with and without considering cell density coefficients and also the average of conventional HI values. * P -values lower than 0.05 represents the statistically significant differences

$$IOE(H) = \left(HI_1 \times \frac{V_1}{V_T} \right) + \left(HI_2 \times \frac{V_2}{V_T} \right) + \left(HI_3 \times \frac{V_3}{V_T} \right) \tag{3}$$

$$IOE(C) = \left(CI_1 \times \frac{V_1}{V_T} \right) + \left(CI_2 \times \frac{V_2}{V_T} \right) + \left(CI_3 \times \frac{V_3}{V_T} \right) \tag{4}$$

$$HI_{mean} = \left(\frac{HI_1 + HI_2 + HI_3}{3} \right) \tag{5}$$

$$CI_{mean} = \left(\frac{CI_1 + CI_2 + CI_3}{3} \right) \tag{6}$$

Statistical analysis

Kolmogorov–Smirnov (K–S) test was used to evaluate the variables’ normality distribution. The results showed that the distributions of the assessed parameters for 20 patients studied in this study were not normal. Therefore, the Wilcoxon statistical analysis was used to evaluate the differences in the relevant indices with considering cell density, without considering cell density and the mean of conventional indices. The significance level in these tests was considered equal to 5%, and the P -values less than 0.05 were considered significant differences. Spearman test was also used to investigate the relationship between IOE indices and radiological parameter (TCP of different targets) values. All of the statistical tests were performed in the SPSS software package Version 22 (SPSS Inc., Chicago, IL, USA).

Results

The mean and standard deviation of HI values for clinical target volumes including CTV_{70Gy}, CTV_{66Gy}, CTV_{60Gy}, and CTV_{53Gy} were 0.086 ± 0.011, 0.078 ± 0.005, 0.151 ± 0.016, 0.105 ± 0.007, respectively. HI values for CTV_{70Gy} and CTV_{66Gy} were lower than the HI values of CTV_{60Gy}, indicating a more homogeneous dose distribution in CTV_{70Gy} and CTV_{66Gy} volumes. Mean and standard deviation values of conformity index (CI) for these CTVs were 0.992 ± 0.005, 0.998 ± 0.004, 0.992 ± 0.004, 0.994 ± 0.004, respectively.

Similar to conventional HI and CI values, IOE (H) values closer to zero indicate the greater effectiveness of the treatment plan. In contrast, IOE (C) values closer to one indicate greater dose painting treatment plan conformity. Figure 2 shows the mean and standard deviation values of the IOE (H) with and without considering cell density coefficients and also the average of conventional HI values. The IOE (H) values with considering cell density had lower values compared to this index without considering cell density. In addition, IOE (C) without considering cell density had higher values compared to this index with considering cell density.

Mean and standard deviation values of IOE (H) with and without considering cell density were 0.05 ± 0.018 and 0.142 ± 0.012, respectively, and show significant differences (P-value = 0.00). Moreover, IOE (H) values showed statistically significant differences from conventional HI values. The results showed that considering cell density in the IOE (H) formula resulted in lower values

than conventional HI and IOE(H) without considering cell density.

Mean and standard deviation values of IOE (C) with and without considering cell density were 0.392 ± 0.124, and 0.993 ± 0.004, respectively (Fig. 3). Furthermore, the mean and standard deviation of conventional CI was 0.994 ± 0.004. The IOE (C) with considering cell density had a significantly lower value compared to conventional CI and IOE (C) without considering cell density (P-value ≤ 0.02).

Correlations between the IOE and tumor control probability values

The mean ± standard deviation values of tumor control probability for CTV_{70Gy} was 94.72 ± 0.65. These values for CTV_{66Gy} and CTV_{60Gy} were 91.58 ± 1.34 and 77.48 ± 3.28 respectively. TCP values greater than 0.7 (70%) have been reported to be "appropriate for total tumor control" in a study by Casares et al. [59].

The Spearman non-parametric correlation was used to investigate the correlation between tumor control probability (TCP), the IOE indices introduced in this study, and conventional HI and CI. The Correlation coefficients between TCP and IOE indices with and without considering cell density were presented in Table 2. Furthermore, the correlation between the TCP and conventional HI and CI values are provided in this table.

The correlation coefficient between TCP and IOE (HI) with considering cell density showed a moderate and negative correlation. IOE (HI) without cell density coefficient was not correlated with tumor control probability. In addition, the correlation coefficient between TCP and IOE (CI) with considering cell density has a moderate and negative correlation. In contrast, the IOE (CI) without cell density coefficient had a strong and positive correlation with TCP. The correlation of TCP with conventional HI mean and CI means were not significant.

Discussion

Dose painting radiotherapy is a technique that can produce more targeted dose delivery to tumor-rich regions while saving organs at risk and critical normal tissues. Dose painting planning would be more complicated

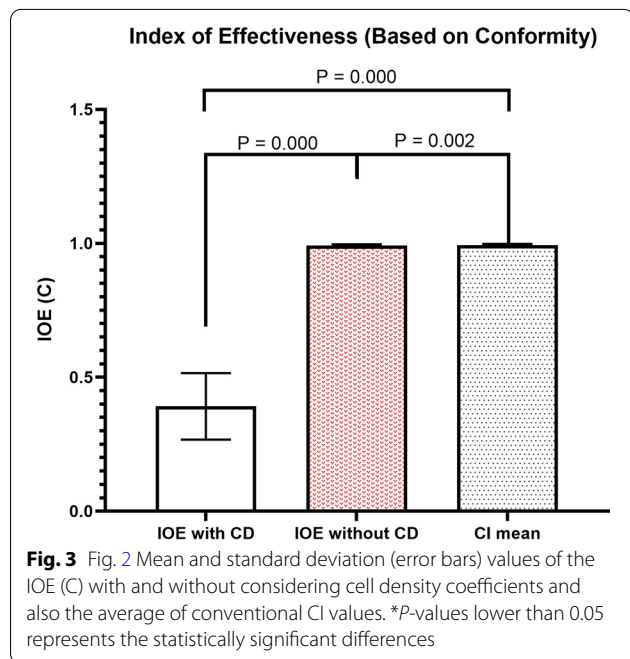


Table 2 The Correlation coefficients between TCP with IOE indices (with and without considering cell density) and conventional plan evaluation indices (HI and CI)

IOE(H) WITH cellular density	IOE(H) WITHOUT cellular density	IOE(C) WITH cellular density	IOE(C) WITHOUT cellular density	HI (mean)	CI (mean)
-0.415	0.152	-0.403	0.624	0.146	0.359

due to different levels of the prescribed dose levels and harder to evaluate with conventional plan quality indices considering uniform dose prescription. Therefore we tried to introduce new indices for evaluating the conformity and homogeneity based on the tumoral cell density and relative volumes of each lesion in prostate IMRT.

There is a recent study [31] tried to introduce new indices to evaluate the plan quality of inhomogeneous irradiated targets and indicate “achievement” in DP plans based on an introduced IOA (index of achievement) as an alternative to the conventional homogeneity index [60]. Their introduced indices may not necessarily be correlated with the biological effect. The proposed indices in this study can be easily modified to incorporate such an effect. We incorporated the tumor cell density obtained from the DWI and ADC images in the plan evaluation indices, and therefore our introduced indices contain the biological effects. However, the cell density can be obtained from other imaging modalities such as “positron emission tomography” and can be evaluated in future studies.

Applying single or just several indices in plan evaluation is an easy and clinically acceptable method. However, using one or several indexes for plan evaluation can suffer from lacking detailed information. Therefore, it must be mentioned that the introduced indices can not replace the standard tools, such as isodose lines and DVH curves evaluation for treatment plan assessment. Although, they can present additional information. There is an alternative to the standard DVH, delta-volume histogram (Δ VH), which was introduced by Witte et al. [30]. They mainly addressed cumulative Δ VH. But in another study by Park et al. [31], an IOA was introduced, which could be supported by differential Δ VH ($d\Delta$ VH). It was assumed that each target voxel has an equal amount of impact on the calculation of plan evaluation metrics. However, the impact of each voxel can be different. For example, under-dose regions in a PTV with a higher prescription dose may have clinically higher risks compared to the under-dose regions in a lower dose PTV. This issue can be resolved by adding voxel-specific or region-specific weighting factors to the previous plan evaluation indices. We used cell density obtained from the ADC map for different PTVs as region-specific weighting factors. We observed that the IOE values based on cellular densities could be completely different when applying the weighting factor. If the biological importance of hotness and coldness becomes much more apparent, a more accurate weighting factor system can be found in the future.

We evaluate the relationship of our proposed indices with TCP. Analytical radiobiological parameters (such

as TCP and normal tissue complication probability (NTCP)) have been widely used for evaluating the quality of treatment plans [61–63]. In particular, several studies proposed TCP models for inhomogeneously irradiated tumors or planning target volumes [18, 64]. Our results showed that IOE(H) with considering cell density and IOE(C) without considering cell density had a stronger relationship with TCP. Therefore it may be concluded that considering cell density values in calculating IOE(C) was not an appropriate idea. However, cell densities must be included in the IOE(H) calculation formula.

The cell density values used in our proposed formula of IOE indices were calculated based on the ADC map. Furthermore, the dose escalation was also based on the regions extracted based on these ADC images. A number of previous studies have advocated the strategy of dose escalation to the imaging-defined targets and dose de-escalation to the rest of the prostate. High dose areas in DP plans can increase the delivery uncertainty due to the limited capability of the treatment planning optimization algorithm to deliver high doses to small and isolated areas. Therefore, these high-dose areas must be defined accurately, and the method of determining these areas must have high repeatability. Comparable findings on the repeatability of ADC features in MRI prostate imaging are reported in the literature. Toivonen et al. [35] reported an ICC of 0.89 for ADC intensity in prostate cancer using MRI, although performed on an ROI basis. Koh et al. also reported high repeatability for ADC measurements in a two-center phase I clinical trial [65].

Van Lin et al. [66] performed a dose painting planning study on five patients with standard whole-prostate RT conventional plan to 78 Gy and a plan with DIL dose escalation to 90 Gy based on dynamic contrast-enhanced and 1H-spectroscopic MRI, and the remainder of the prostate dose de-escalation to 70 Gy. They reported that both plans had similar TCPs; however, the dose painting had lower NTCPs. In another study by Seppala et al. [21], a planning study of 12 patients was performed with DILs defined based on 11 C acetate PET scans. Six different dose escalation plans were performed and compared for each patient, including a whole-prostate RT plan to 77.9 Gy, and DIL dose escalations to 77.9 Gy, 81 Gy, 84 Gy, 87 Gy and 90 Gy, with remaining prostate dose de-escalations to 72 Gy. They reported that the dose painting plans had higher TCP values compared with the standard whole-prostate plan and that the highest probability of tumor control without complication was related to a plan with an average dose of 82.1 Gy to the DIL. In a study by Chang et al. [23] the technical feasibility of IMRT dose painting using 11 C-choline PET scans were evaluated in eight patients with localized prostate cancer. Two DILs were defined including 60% and 70% of the maximum

standardized uptake values ($SUV_{60\%}$ and $SUV_{70\%}$). Three IMRT plans were designed including: PLAN₇₈ (whole-prostate irradiation with 78 Gy); PLAN₇₈₋₉₀ (whole-prostate RT to 78 Gy, a boost to the $SUV_{60\%}$ and $SUV_{70\%}$ to 84 Gy, and 90 Gy, respectively); and PLAN₇₂₋₉₀ (whole-prostate RT to 72 Gy, a boost to the $SUV_{60\%}$ and $SUV_{70\%}$ to 84 Gy, and 90 Gy, respectively). TCP based on PET scan-defined volumes (TCP_{PET}) and on prostatectomy-defined volumes (TCP_{path}), and rectal NTCP were compared between the plans. They reported that both dose painting plans (PLAN₇₈₋₉₀ and PLAN₇₂₋₉₀) had significantly higher TCP_{PET} and TCP_{path} values than conventional IMRT plan (PLAN₇₈), without significant differences in TCP_{PET} or TCP_{path} between dose painting plans. Furthermore, There were no significant differences in rectal NTCPs between the 3 plans.

We used rigid image registration for fusing CT and MRI images. Deformable registration can also be used for this purpose. Rigid registration is very effective in cases when no anatomic change is expected [67]. In our study, patients underwent MR imaging after CT imaging in one day with a maximum delay of one hour. Their positioning was similar in both imaging and therefore, we don't expect significant anatomical changes between the imaging techniques. If there is a big time gap between CT and MR imaging, patients might experience anatomical changes due to tumor shrinkage/growth, weight loss, or physiological organ shape variations. In these cases deformable registration can manage the distortion between two image sets and provide superior results [68–70]. In comparison to rigid registration, deformable registration has a significantly greater degrees of freedom [67], and can deform the image and structures with different algorithms (such as intensity-based approaches, landmark-based thin-plate spline, or biophysical and finite element modelling-based registration) (67).

This study has some limitations, and several factors must be addressed before clinically adopting this strategy. First, deformable registration might be superior in cases with the significant time intervals between CT and MR imaging because this could deal with changes in the prostate shape and discrepancies in the prostate size between imaging modalities more adequately than was possible using rigid registration. Second, the proposed plan evaluation indices in this study, including IOE(H) and IOE(c) with and without considering cell densities, must be assessed for a bigger group of patients and also in other cancer sites.

Conclusions

New IOE dose painting plan evaluation indices proposed in this study have simple calculation methods and incorporate cellular density as an index of lesion importance

obtained from MRI ADC images for prostate cancer IMRT. These indices can be used for evaluating prostate IMRT dose painting plans. Cell densities must be considered in the IOE(H) (calculation formula, and it's more appropriate to calculate IOE(C) without considering cell density.

Abbreviations

IMRT: Intensity modulated radiotherapy; VMAT: Volumetric modulated arc therapy; IMAT: Intensity modulated arc therapy; ADC: Apparent diffusion coefficient; GTV: Gross tumor volume; CTV: Clinical tumor volume; PTV: Planning tumor volume; HI: Homogeneity index; CI: Conformity index; IOE: Index of effectiveness; DVH: Dose volume histogram; MRI: Magnetic resonance imaging; CT: Computed tomography.

Supplementary Information

The online version contains supplementary material available at <https://doi.org/10.1186/s13014-022-02163-7>.

Additional file 1. An in-house MATLAB program developed to automatically identify lesion regions on ADC images based on ADC values.

Acknowledgements

We like to express our appreciation to Shohadaye Tajrish hospital (Tehran, Iran) for allowing us to use their software and devices. In addition, we appreciate to all the patients permit us to use their medical images and informations for performing this research.

Author contributions

Bijan Hashemi was responsible for the study conception, design, acquisition of data, and finalizing of the manuscript. All the authors contributed to data analyzing and writing the manuscript draft. Furthermore, all the authors read and approved the final manuscript.

Funding

This work had not any funds or grant from any institution.

Availability of data and materials

All data obtained during the current study are available from the corresponding author on reasonable request.

Declarations

Ethics approval and consent to participate

This retrospective study was performed in accordance with the relevant guidelines and regulations and the methods of this study have been approved by the National Ethics Committee. All the patients (or one of his/her family member) whom their medical images were used in our study were aware of using their images in this study.

Consent for publication

All the authors consent to publish the manuscript in *Radiation Oncology*.

Competing interests

The authors declare no conflict of interest.

Author details

¹Department of Medical Physics, Faculty of Medical Sciences, Tarbiat Modares University, Tehran 1411713116, Iran. ²Department of Radiology Technology, Faculty of Allied Medical Sciences, Shahid Beheshti University of Medical Sciences, Tehran 1985717443, Iran. ³Department of Radiation Oncology, Faculty of Medicine, Shahid Beheshti University of Medical Sciences, Tehran 1985717443, Iran.

Received: 1 August 2022 Accepted: 17 November 2022
Published online: 23 November 2022

References

- Khan FM, Sperduto PW, Gibbons JP. Khan's treatment planning in radiation oncology. Philadelphia: Lippincott Williams & Wilkins; 2021.
- Tsai CL, Wu JK, Chao HL, Tsai YC, Cheng JCH. Treatment and dosimetric advantages between VMAT, IMRT, and helical tomotherapy in prostate cancer. *Med Dosim*. 2011;36(3):264–71.
- Hardcastle N, Tomé WA, Foo K, Miller A, Carolan M, Metcalfe P. Comparison of prostate IMRT and VMAT biologically optimised treatment plans. *Med Dosim*. 2011;36(3):292–8.
- Kuban DA, Tucker SL, Dong L, Starkschall G, Huang EH, Cheung MR, et al. Long-term results of the MD Anderson randomized dose-escalation trial for prostate cancer. *Int J Radiat Oncol Biol Phys*. 2008;70(1):67–74.
- Shipley WU, Verhey LJ, Munzenrider JE, Suit HD, Urie MM, McManus PL, et al. Advanced prostate cancer: the results of a randomized comparative trial of high dose irradiation boosting with conformal protons compared with conventional dose irradiation using photons alone. *Int J Radiat Oncol Biol Phys*. 1995;32(1):3–12.
- Beckendorf V, Guerif S, Le Prisé E, Cosset JM, Bougnoux A, Chauvet B, et al. 70 Gy versus 80 Gy in localized prostate cancer: 5-year results of GETUG 06 randomized trial. *Int J Radiat Oncol Biol Phys*. 2011;80(4):1056–63.
- Al-Mamgani A, van Putten WL, van der Wielen GJ, Levendag PC, Incrocci L. Dose escalation and quality of life in patients with localized prostate cancer treated with radiotherapy: long-term results of the Dutch randomized dose-escalation trial (CKTO 96–10 trial). *Int J Radiat Oncol Biol Phys*. 2011;79(4):1004–12.
- Peeters ST, Heemsbergen WD, Koper PC, Van Putten WL, Slot A, Dielwart MF, et al. Dose-response in radiotherapy for localized prostate cancer: results of the Dutch multicenter randomized phase III trial comparing 68 Gy of radiotherapy with 78 Gy. *J Clin Oncol*. 2006;24(13):1990–6.
- Deanaley DP, Sydes MR, Graham JD, Aird EG, Bottomley D, Cowan RA, et al. Escalated-dose versus standard-dose conformal radiotherapy in prostate cancer: first results from the MRC RT01 randomised controlled trial. *Lancet Oncol*. 2007;8(6):475–87.
- Zietman AL, DeSilvio ML, Slater JD, Rossi CJ, Miller DW, Adams JA, et al. Comparison of conventional-dose vs high-dose conformal radiation therapy in clinically localized adenocarcinoma of the prostate: a randomized controlled trial. *JAMA*. 2005;294(10):1233–9.
- Hanks GE, Hanlon AL, Schultheiss TE, Pinover WH, Movsas B, Epstein BE, et al. Dose escalation with 3D conformal treatment: five year outcomes, treatment optimization, and future directions. *Int J Radiat Oncol Biol Phys*. 1998;41(3):501–10.
- Zelevsky M, Leibel S, Gaudin P, Kutcher G, Fleshner N, Venkatraman ES, et al. Dose escalation with three-dimensional conformal radiation therapy affects the outcome in prostate cancer. *Int J Radiat Oncol Biol Phys*. 1998;41(3):491–500.
- Rezaeijoo SM, Hashemi B, Mofid B, Bakhshandeh M, Mahdavi A, Hashemi MS. The feasibility of a dose painting procedure to treat prostate cancer based on mpMR images and hierarchical clustering. *Radiat Oncol*. 2021;16(1):1–16.
- Viani GA, Stefano EJ, Afonso SL. Higher-than-conventional radiation doses in localized prostate cancer treatment: a meta-analysis of randomized, controlled trials. *Int J Radiat Oncol Biol Phys*. 2009;74(5):1405–18.
- Ghai S, Haider MA. Multiparametric-MRI in diagnosis of prostate cancer. *Indian J Urol IJU J Urol Soc India*. 2015;31(3):194.
- Jomehzadeh A, Shokrani P, Mohammadi M, Amouheidari A. A quality assurance program for an amorphous silicon electronic portal imaging device using in-house developed phantoms: a method development for dosimetry purposes. 2014.
- Skyt PS, Petersen JB, Yates ES, Poulsen PR, Ravkilde TL, Balling P, et al. Dosimetric verification of complex radiotherapy with a 3D optically based dosimetry system: dose painting and target tracking. *Acta Oncol*. 2013;52(7):1445–50.
- Marks LB, Yorke ED, Jackson A, Ten Haken RK, Constine LS, Eisbruch A, et al. Use of normal tissue complication probability models in the clinic. *Int J Radiat Oncol Biol Phys*. 2010;76(3):S10–9.
- Barentsz JO, Richenberg J, Clements R, Choyke P, Verma S, Villeirs G, et al. ESUR prostate MR guidelines 2012. *Eur Radiol*. 2012;22(4):746–57.
- Dickinson L, Ahmed HU, Allen C, Barentsz JO, Carey B, Futterer JJ, et al. Scoring systems used for the interpretation and reporting of multiparametric MRI for prostate cancer detection, localization, and characterization: could standardization lead to improved utilization of imaging within the diagnostic pathway? *J Magn Reson Imaging*. 2013;37(1):48–58.
- Seppälä J, Seppänen M, Arponen E, Lindholm P, Minn H. Carbon-11 acetate PET/CT based dose escalated IMRT in prostate cancer. *Radiother Oncol*. 2009;93(2):234–40.
- Niyazi M, Bartenstein P, Belka C, Ganswindt U. Choline PET based dose-painting in prostate cancer-Modelling of dose effects. *Radiat Oncol*. 2010;5(1):1–9.
- Chang JH, Joon DL, Lee ST, Gong SJ, Anderson NJ, Scott AM, et al. Intensity modulated radiation therapy dose painting for localized prostate cancer using 11C-choline positron emission tomography scans. *Int J Radiat Oncol Biol Phys*. 2012;83(5):e691–6.
- Thorwarth D, Geets X, Paiusco M. Physical radiotherapy treatment planning based on functional PET/CT data. *Radiother Oncol*. 2010;96(3):317–24.
- Vos PC, Barentsz JO, Karssemeijer N, Huisman HJ. Automatic computer-aided detection of prostate cancer based on multiparametric magnetic resonance image analysis. *Phys Med Biol*. 2012;57(6):1527.
- Viswanath SE, Bloch NB, Chappelow JC, Toth R, Profsky NM, Genega EM, et al. Central gland and peripheral zone prostate tumors have significantly different quantitative imaging signatures on 3 Tesla endorectal, in vivo T2-weighted MR imagery. *J Magn Reson Imaging*. 2012;36(1):213–24.
- Dinh CV, Steenbergen P, Ghobadi G, Heijmink SW, Pos FJ, Haustermans K, et al. Magnetic resonance imaging for prostate cancer radiotherapy. *Phys Med*. 2016;32(3):446–51.
- Dinh CV, Steenbergen P, Ghobadi G, van der Poel H, Heijmink SW, de Jong J, et al. Multicenter validation of prostate tumor localization using multiparametric MRI and prior knowledge. *Med Phys*. 2017;44(3):949–61.
- Groenendaal G, Borren A, Moman MR, Monnikhof E, Van Diest PJ, Philippens ME, et al. Pathologic validation of a model based on diffusion-weighted imaging and dynamic contrast-enhanced magnetic resonance imaging for tumor delineation in the prostate peripheral zone. *Int J Radiat Oncol Biol Phys*. 2012;82(3):e537–44.
- Witte M, Shakirin G, Houweling A, Peulen H, van Herk M. Dealing with geometric uncertainties in dose painting by numbers: introducing the ΔV_H . *Radiother Oncol*. 2011;100(3):402–6.
- Park YK, Park S, Wu HG, Kim S. A new plan quality index for dose painting radiotherapy. *J Appl Clin Med Phys*. 2014;15(4):316–25.
- Yoon M, Park SY, Shin D, Lee SB, Pyo HR, Kim DY, et al. A new homogeneity index based on statistical analysis of the dose–volume histogram. *J Appl Clin Med Phys*. 2007;8(2):9–17.
- Dogan N, King S, Emami B, Mohideen N, Mirkovic N, Leybovich LB, et al. Assessment of different IMRT boost delivery methods on target coverage and normal-tissue sparing. *Int J Radiat Oncol Biol Phys*. 2003;57(5):1480–91.
- Szafer A, Zhong J, Anderson AW, Gore JC. Diffusion-weighted imaging in tissues: theoretical models. *NMR Biomed*. 1995;8(7):289–96.
- Toivonen J, Merisaari H, Pesola M, Taimen P, Boström PJ, Pahikkala T, et al. Mathematical models for diffusion-weighted imaging of prostate cancer using b values up to 2000 s/mm²: Correlation with Gleason score and repeatability of region of interest analysis. *Magn Reson Med*. 2015;74(4):1116–24.
- Hentschel B, Oehler W, Strauß D, Ulrich A, Malich A. Definition of the CTV prostate in CT and MRI by using CT–MRI image fusion in IMRT planning for prostate cancer. *Strahlenther Onkol*. 2011;187(3):183–90.
- Thörmer G, Otto J, Reiss-Zimmermann M, Seiwerts M, Moche M, Garnov N, et al. Diagnostic value of ADC in patients with prostate cancer: influence of the choice of b values. *Eur Radiol*. 2012;22(8):1820–8.
- Pepe P, D'urso D, Garufi A, Priolo G, Pennisi M, Russo G, et al. Multiparametric MRI apparent diffusion coefficient (ADC) accuracy in diagnosing clinically significant prostate cancer. *In Vivo*. 2017;31(3):415–8.
- Jereczek-Fossa BA, Santoro L, Zerini D, Fodor C, Vischioni B, Dispinzieri M, et al. Image guided hypofractionated radiotherapy and quality of life for

- localized prostate cancer: prospective longitudinal study in 337 patients. *J Urol.* 2013;189(6):2099–103.
40. Banaei A, Hashemi B, Bakhshandeh M, Mofid B. Comparison of dosimetric and radiobiological effects of various IMRT techniques regarding to joint volume between target tissue and organs at risk in prostate cancer patients. *Tehran Univ Med J.* 2019;77(2):92–100.
 41. Banaei A, Hashemi B, Bakhshandeh M, Mofid B. Evaluation of various common prostate IMRT techniques based on estimated tumor control and normal tissue complication probabilities in correlation with patients anatomical parameters derived from the CT scans. *Pol J Med Phys Eng.* 2019;25(1):35–41.
 42. Banaei A, Hashemi B, Bakhshandeh M, Mofid B. Trade-off between the conflicting planning goals in correlation with patient's anatomical parameters for intensity-modulated radiotherapy of prostate cancer patients. *J Radiother Pract.* 2019;18(3):232–8.
 43. Cozzarini C, Fiorino C, Deantoni C, Briganti A, Fodor A, La Macchia M, et al. Higher-than-expected severe (Grade 3–4) late urinary toxicity after postprostatectomy hypofractionated radiotherapy: a single-institution analysis of 1176 patients. *Eur Urol.* 2014;66(6):1024–30.
 44. Jereczek-Fossa BA, Surgo A, Maisonneuve P, Maucieri A, Gerardi MA, Zerini D, et al. Late toxicity of image-guided hypofractionated radiotherapy for prostate: non-randomized comparison with conventional fractionation. *Radiol Med (Torino).* 2019;124(1):65–78.
 45. Avkshol V, Ruth KJ, Ross EA, Hallman MA, Greenberg RE, Price RA Jr, et al. Ten-year update of a randomized, prospective trial of conventional fractionated versus moderate hypofractionated radiation therapy for localized prostate cancer. *J Clin Oncol.* 2020;38(15):1676.
 46. Jereczek-Fossa BA, Zerini D, Fodor C, Santoro L, Cambria R, Garibaldi C, et al. Acute toxicity of image-guided hypofractionated radiotherapy for prostate cancer: nonrandomized comparison with conventional fractionation. In: *Urologic Oncology: Seminars and Original Investigations.* New York: Elsevier; 2011. p. 523–32.
 47. Ricardi U, Franco P, Munoz F, Levis M, Fiandra C, Guarneri A, et al. Three-dimensional ultrasound-based image-guided hypofractionated radiotherapy for intermediate-risk prostate cancer: results of a consecutive case series. *Cancer Invest.* 2015;33(2):23–8.
 48. Onjukka E, Uzan J, Baker C, Howard L, Nahum A, Syndikus I. Twenty fraction prostate radiotherapy with intra-prostatic boost: results of a pilot study. *Clin Oncol.* 2017;29(1):6–14.
 49. Uzan J, Nahum AE, Syndikus I. Prostate dose-painting radiotherapy and radiobiological guided optimisation enhances the therapeutic ratio. *Clin Oncol.* 2016;28(3):165–70.
 50. Pollack A, Walker G, Horwitz EM, Price R, Feigenberg S, Konski AA, et al. Randomized trial of hypofractionated external-beam radiotherapy for prostate cancer. *J Clin Oncol.* 2013;31(31):3860.
 51. Shende R, Gupta G, Patel G, Kumar S. Assessment and performance evaluation of photon optimizer (PO) vs. dose volume optimizer (DVO) for IMRT and progressive resolution optimizer (PRO) for RapidArc planning using a virtual phantom. *Int J Cancer Ther Oncol.* 2016;4(3):437.
 52. Lee T, Hammad M, Chan TC, Craig T, Sharpe MB. Predicting objective function weights from patient anatomy in prostate IMRT treatment planning. *Med Phys.* 2013;40(12):121706.
 53. Hasenbalg F, Neuenschwander H, Mini R, Born EJ. Collapsed cone convolution and analytical anisotropic algorithm dose calculations compared to VMC++ Monte Carlo simulations in clinical cases. *Phys Med Biol.* 2007;52(13):3679.
 54. Gagné IM, Zavgorodni S. Evaluation of the analytical anisotropic algorithm in an extreme water–lung interface phantom using Monte Carlo dose calculations. *J Appl Clin Med Phys.* 2007;8(1):33–46.
 55. Van Esch A, Tillikainen L, Pyykkonen J, Tenhunen M, Helminen H, Siljamäki S, et al. Testing of the analytical anisotropic algorithm for photon dose calculation. *Med Phys.* 2006;33(11):4130–48.
 56. Sanchez-Nieto B, Nahum AE. BIOPLAN: software for the biological evaluation of radiotherapy treatment plans. *Med Dosim.* 2000;25(2):71–6.
 57. Zaider M, Hanin L. Tumor control probability in radiation treatment. *Med Phys.* 2011;38(2):574–83.
 58. Deb P, Fielding A. Radiobiological model comparison of 3D conformal radiotherapy and IMRT plans for the treatment of prostate cancer. *Australas Phys Eng Sci Med.* 2009;32(2):51–61.
 59. Casares-Magaz O, van der Heide UA, Rørvik J, Steenbergen P, Muren LP. A tumour control probability model for radiotherapy of prostate cancer using magnetic resonance imaging-based apparent diffusion coefficient maps. *Radiother Oncol.* 2016;119(1):111–6.
 60. Kataria T, Sharma K, Subramani V, Karthick KP, Bisht SS. Homogeneity index: an objective tool for assessment of conformal radiation treatments. *J Med Physics Association Med Phys India.* 2012;37(4):207.
 61. Adkison JB, Khuntia D, Bentzen SM, Cannon GM, Tome WA, Jaradat H, et al. Dose escalated, hypofractionated radiotherapy using helical tomotherapy for inoperable non-small cell lung cancer: preliminary results of a risk-stratified phase I dose escalation study. *Technol Cancer Res Treat.* 2008;7(6):441–7.
 62. Warkentin B, Stavrev P, Stavreva N, Field C, Fallone BG. A TCP-NTCP estimation module using DVHs and known radiobiological models and parameter sets. *J Appl Clin Med Phys.* 2004;5(1):50–63.
 63. Rosenzweig KE, Fox JL, Yorke E, Amols H, Jackson A, Rusch V, et al. Results of a phase I dose-escalation study using three-dimensional conformal radiotherapy in the treatment of inoperable nonsmall cell lung carcinoma. *Cancer Interdiscip Int J Am Cancer Soc.* 2005;103(10):2118–27.
 64. Goitein M, Niemierko A. Intensity modulated therapy and inhomogeneous dose to the tumor: a note of caution. *Int J Radiat Oncol Biol Phys.* 1996;36(2):519–22.
 65. Koh DM, Blackledge M, Collins DJ, Padhani AR, Wallace T, Wilton B, et al. Reproducibility and changes in the apparent diffusion coefficients of solid tumours treated with combretastatin A4 phosphate and bevacizumab in a two-centre phase I clinical trial. *Eur Radiol.* 2009;19(11):2728–38.
 66. van Lin EN, Fütterer JJ, Heijmink SW, van der Vight LP, Hoffmann AL, van Kollenburg P, et al. IMRT boost dose planning on dominant intraprostatic lesions: gold marker-based three-dimensional fusion of CT with dynamic contrast-enhanced and 1H-spectroscopic MRI. *Int J Radiat Oncol Biol Phys.* 2006;65(1):291–303.
 67. Oh S, Kim S. Deformable image registration in radiation therapy. *Radiat Oncol J.* 2017;35(2):101.
 68. Kashani R, Hub M, Balter JM, Kessler ML, Dong L, Zhang L, et al. Objective assessment of deformable image registration in radiotherapy: a multi-institution study. *Med Phys.* 2008;35(12):5944–53.
 69. Kashani R, Hub M, Kessler ML, Balter JM. A physical phantom for assessment of accuracy of deformable alignment algorithms. *Med Phys.* 2007;34(7):2785–8.
 70. Pukala J, Johnson PB, Shah AP, Langen KM, Bova FJ, Staton RJ, et al. Benchmarking of five commercial deformable image registration algorithms for head and neck patients. *J Appl Clin Med Phys.* 2016;17(3):25–40.

Publisher's Note

Springer Nature remains neutral with regard to jurisdictional claims in published maps and institutional affiliations.

Ready to submit your research? Choose BMC and benefit from:

- fast, convenient online submission
- thorough peer review by experienced researchers in your field
- rapid publication on acceptance
- support for research data, including large and complex data types
- gold Open Access which fosters wider collaboration and increased citations
- maximum visibility for your research: over 100M website views per year

At BMC, research is always in progress.

Learn more biomedcentral.com/submissions

